Cascade developer meeting

hope you all had a good start into 2023 !

TMDlib: inclusion of Pavia sets

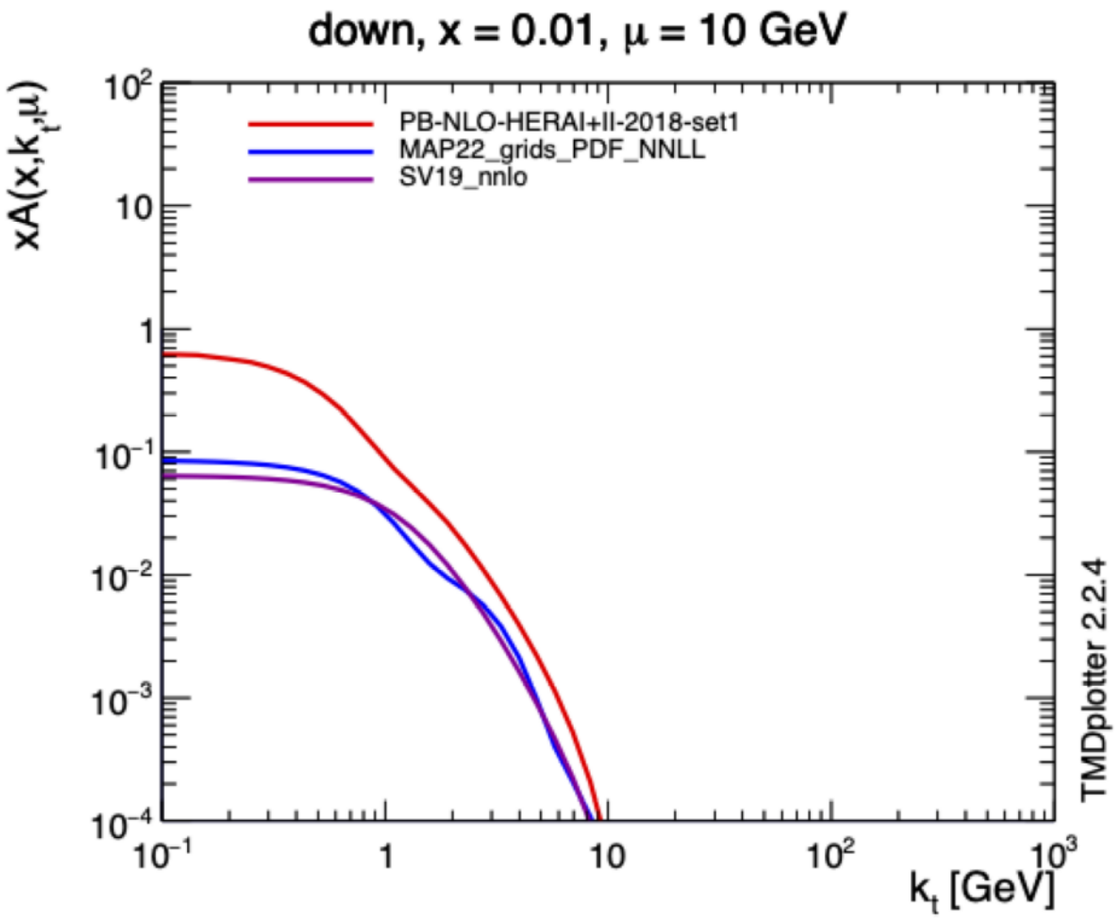

- Where is the difference in normalization coming from ?
  - Alessandro:

$$\int d^2 p_T TMD1$$

$$= 2\pi \int p_T dp_T TMD1$$

$$= PDF$$

- This is what I would call the "standard" definition, while I believe the PB grids are done based on a slightly different definition

$$\int p_T dp_T TMD2 = PDF.$$

CASCADE news

- New version ready: 3.3.1
  - timing and Maxfactor
    - tested: significant increase in speed (and simplicity)
  - new version released in git and hepforge

New papers

- new papers in pipeline
  - The small kt region in the parton branching approach and relation to CSS
    - this paper will be different:
      - small author list of Antwerp people including Mikel
      - no longer CASCADE group paper

New papers

- The small kt region in DY production at NLO with the parton branching method
  - phneno applications, determination of intrinsic kt
  - determine qs as fct of m_DY at 13 TeV
  - determine qs as fct of m_DY at 8 TeV ?
  - if all goes smooth also at low m_DY and low energy
    - all fits should be treating stat and syst uncertainties different, as proposed by LHCEW working group
- This paper is open and will stay open:
  - Please reply to me, if you want to be co-author, after reading and commenting

Intrinsic kt and soft region

version 3.0
February 7, 2023

The small k_T region in Drell-Yan production at next-to-leading order with the Parton Branching Method

I. Bubanja[1,2], A. Bermudez Martinez[3], L.I. Estevez Banos[3], L. Favart[2], F. Guzman[4], H. Jung[3,5], M. Mendizabal[3], K. Moral Figueroa[3], N. Raicevic[1], M. Seidel[6], S. Taheri Monfared[3], K. Wichmann[3], Q. Wang[3,7], and H. Yang[3,7]

[1]Faculty of Natural sciences and Mathematics, University of Montenegro, Podgorica, Montenegro
[2]Interuniversity Institute for High Energies (IIHE), Université libre de Bruxelles, Belgium
[3]Deutsches Elektronen-Synchrotron DESY, Hamburg, Germany
[4]InSTEC, Universidad de La Habana, Havanna, Cuba
[5]II. Institut für Theoretische Physik, Universität Hamburg, Hamburg, Germany
[6]Riga Technical University, Riga, Latvia
[7]School of Physics, Peking University, Beijing, China

The CASCADE group

leads to a small contribution of pure of intrinsic k_T, while most of the small k_T-contribution is already treated within the PB-calculation. We also show, that the proper treatment of photon radiation from the DY decay leptons is rather important, especially in the DY mass region below the Z boson peak. The contribution of intrinsic k_T of heavy flavor partons is negligible over the whole range, since heavy quarks are not present in the initial configuration of the proton.

2 PB TMDs

The PB method [4, 5] provides a solution of the DGLAP [13–16] evolution equations. The DGLAP evolution equation for the parton density of parton a with momentum fraction x at the scale μ reads:

$$\mu^2 \frac{\partial f_a(x,\mu^2)}{\partial \mu^2} = \sum_b \int_x^1 \frac{dz}{z} P_{ab}\left(\alpha_s(\mu^2), z\right) \; f_b\left(\frac{x}{z}, \mu^2\right) \; , \tag{1}$$

with the regularized DGLAP splitting functions P_{ab} describing the splitting of parton b into a parton a. P_{ab} can be decomposed as (in the notation of Ref. [4]):

$$P_{ab}(z,\alpha_s) = D_{ab}(\alpha_s)\delta(1-z) + K_{ab}(\alpha_s)\frac{1}{(1-z)_+} + R_{ab}(z,\alpha_s) \; . \tag{2}$$

The coefficients D and K can be written as $D_{ab}(\alpha_s) = \delta_{ab} d_a(\alpha_s)$, $K_{ab}(\alpha_s) = \delta_{ab} k_a(\alpha_s)$ and the coefficients R_{ab} contain only terms which are not singular for $z \to 1$. Each of those three coefficients can be expanded in powers of α_s:

$$d_a(\alpha_s) = \sum_{n=1}^{\infty} \left(\frac{\alpha_s}{2\pi}\right)^n d_a^{(n-1)}, \; k_a(\alpha_s) = \sum_{n=1}^{\infty} \left(\frac{\alpha_s}{2\pi}\right)^n k_a^{(n-1)}, \; R_{ab}(z,\alpha_s) = \sum_{n=1}^{\infty} \left(\frac{\alpha_s}{2\pi}\right)^n R_{ab}^{(n-1)}(z) \tag{3}$$

The plus-prescription and the D part in eq.(2) can be expanded by introducing a Sudakov form factor $\Delta_a^S(\mu^2)$ (see e.g. [17]), which is defined as:

$$\Delta_a^S(\mu^2, \mu_0^2) = \exp\left(-\int_{\mu_0^2}^{\mu^2} \frac{\mathrm{d}\mu'^2}{\mu'^2}\left[\int_0^{z_M} k_a(\alpha_s)\frac{1}{1-z}\mathrm{d}z - d_a(\alpha_s)\right]\right) \; . \tag{4}$$

An upper limit $z_M = 1-\epsilon$ is introduced to allow numerical integration over z, and $\epsilon \to 0$ is required to reproduce DGLAP. Note, that the expression of Δ_a^S is different from the one used in Ref. [4], since the full unregularized splitting function, including virtual contributions, is used.

The evolution equation for the parton density $f_a(x,\mu^2)$ at scale μ is then given by:

$$f_a(x,\mu^2) = \Delta_a^S(\mu^2)\, f_a(x,\mu_0^2) + \sum_b \int_{\mu_0^2}^{\mu^2} \frac{d\mu'^2}{\mu'^2} \frac{\Delta_a^S(\mu^2)}{\Delta_a^S(\mu'^2)} \int_x^{z_M} \frac{dz}{z} \; \hat{P}_{ab}(\alpha_s(\mu'^2), z) \; f_b\left(\frac{x}{z}, \mu'^2\right) \tag{5}$$

Intrinsic kt and soft region

with the unregularized splitting functions $\hat{P}_{ab}$ (replacing $1/(1-z)_+$ by $1/(1-z)$) and μ_0 being the starting scale.

Equation eq.(5) can be easily extended for transverse momentum dependent parton densities, following the same arguments given in Ref. [4]:

$$\begin{aligned}\mathcal{A}_a(x,\mathbf{k},\mu^2) &= \Delta_a^S(\mu^2)\,\mathcal{A}_a(x,\mathbf{k},\mu_0^2) + \int \frac{d^2\mathbf{q}'}{\pi\mathbf{q}'^2}\,\frac{\Delta_a^S(\mu^2)}{\Delta_a^S(\mathbf{q}'^2)}\,\Theta(\mu^2-\mathbf{q}'^2)\,\Theta(\mathbf{q}'^2-\mu_0^2) \\ &\times \left[\int_x^{z_M}\frac{dz}{z}\,\hat{P}_{ab}(\alpha_s(\mathbf{q}'^2),z)\,\mathcal{A}_a\left(\frac{x}{z},\mathbf{k}+(1-z)\mathbf{q}',\mathbf{q}'^2\right)\right]\,, \qquad (6)\end{aligned}$$

where $\mathbf{k}$ and $\mathbf{q}'$ are 2-dimensional transverse momentum vectors.

2.1 The PB sudakov form factor

The concept of resolvable and non-resolvable branchings with Sudakov form factors allows for an intuitive interpretation of the parton evolution pattern. The Sudakov form factors give the probability to evolve from one scale to another without resolvable branching. While the concept of the PB method is similar to a parton shower approach, the method is used here to solve the DGLAP evolution equation.

Since the Sudakov form factor Δ_a^S contains also the region of very soft gluon emissions ($z \to 1$), it is of advantage to split Δ_a^S into a perturbative ($q_t > q_0$) and non-perturbative ($q_t < q_0$) part by introducing a resolution scale $z_{\rm dyn} = 1 - q_0/\mu'$. This scale is motivated from angular ordering and the requirement to resolve an emitted parton with transverse momentum $q_t > q_0$.

The Sudakov form factor is then given by:

$$\begin{aligned}\Delta_a(\mu^2,\mu_0^2) = &\quad \exp\left(-\int_{\mu_0^2}^{\mu^2}\frac{d\mu'^2}{\mu'^2}\left[\int_0^{z_{\rm dyn}(\mu')}dz\,\frac{k_a(\alpha_s)}{1-z} - d_a(\alpha_s)\right]\right) \\ &\times\exp\left(-\int_{\mu_0^2}^{\mu^2}\frac{d\mu'^2}{\mu'^2}\int_{z_{\rm dyn}(\mu')}^{z_M}dz\,\frac{k_a(\alpha_s)}{1-z}\right) \\ = &\quad \Delta_a^{(\rm P)}\left(\mu^2,\mu_0^2,q_0^2\right)\cdot\Delta_a^{(\rm NP)}\left(\mu^2,\mu_0^2,\epsilon,q_0^2\right)\,, \qquad (7)\end{aligned}$$

It can be shown, as a side effect, that $\Delta_a^{(\rm P)}$ coincides with the Sudakov form factor used in CSS [1] (for a detailed description see [18]) up to next-to-leading and even partially next-to-next-to-leading logarithms. The non-perturbative Sudakov form factor $\Delta_a^{(\rm NP)}$ has exactly the same structure as the non-perturbative Sudakov form factor in CSS: under certain assumptions, the z-integral can be performed, and a $\log(\mu^2/\mu_0^2)$ appears. With the description of Δ_a^S in eq.(7) the non-perturbative Sudakov form factor can be calculated and finds a natural explanation in PB as coming from the proper treatment of the soft region.

On a collinear level, it was shown in Ref. [4] that the PB-approach reproduces exactly the DGLAP evolution of parton densities, if the argument in α_s is the evolution scale and

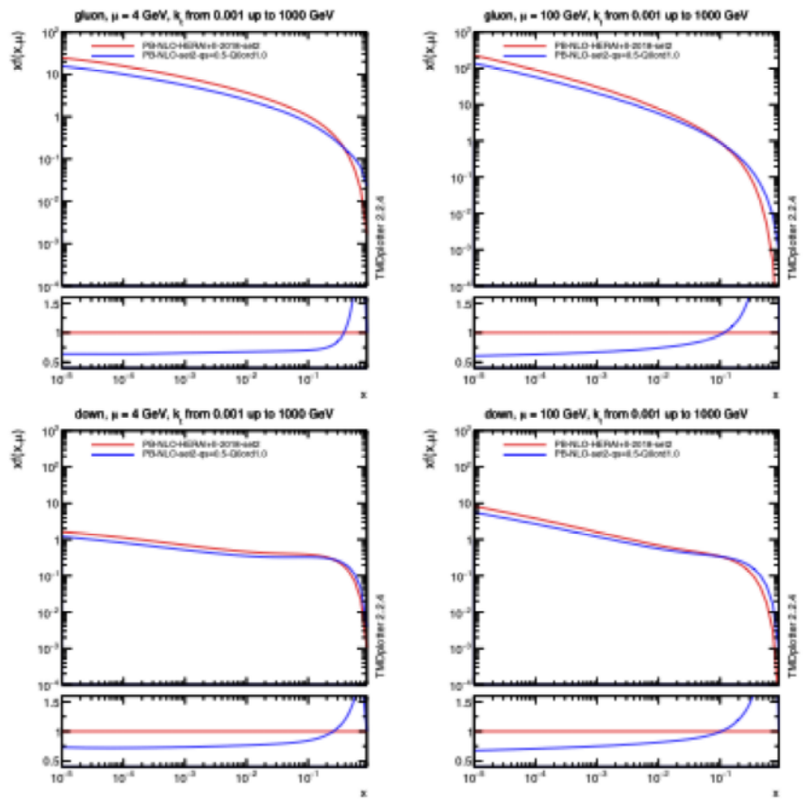

Figure 1: Integrated gluon and down-quark distributions at $\mu = 4$ GeV (left column) and $\mu = 100$ GeV (right column) obtained from the PB approach for different values of z_M: PB-NLO-2018 set2 applies $z_M \to 1$ and PB-NLO-set2 applies $z_M = z_{\rm dyn}$. The ratio plots show the ratios to the one for $z_M \to 1$.

distribution of partons inside the proton. In Fig. 3 we show a comparison of the transverse momentum distributions for PB-NLO-2018 set1 and PB-NLO-2018 set2 and compare it with the scenario when there is no intrinsic $k_{\rm T}$ distribution included (practically the intrinsic $k_{\rm T}$ distribution is generated from a Gauss distribution with very small width $q_s = \sqrt{2}\sigma = 0.0001$ GeV). A huge difference between set1 and set2 without any intrinsic $k_{\rm T}$-distribution is observed, which is coming from the treatment of very soft gluons ($z \to 1$), since the transverse

Intrinsic kt and soft region

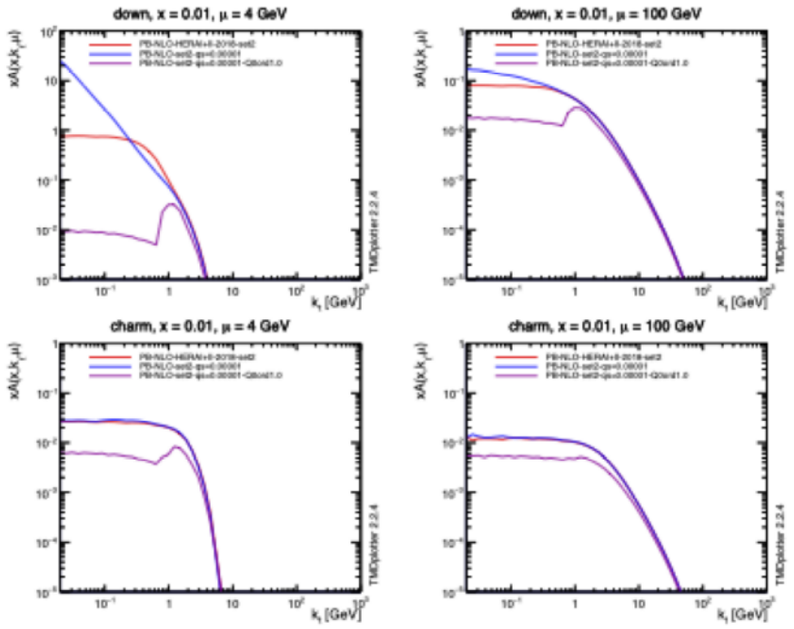

Figure 2: Transverse momentum distributions down- and charm quarks at $\mu = 4$ GeV (left column) and $\mu = 100$ GeV (right column) obtained from the PB approach for $z_M \to 1$ as well as $z_M = z_{\rm dyn} = 1 - q_0/q$. The blue and magenta curves (labelled $qs = 0.00001$) have no intrinsic $k_{\rm T}$ distribution included.

momentum is calculated from $k_{\rm T} = (1-z)q_t$, whit $q_t = \sqrt{\mathbf{q}^2}$ being the transverse momentum of the emitted parton with $q_t > \mu_0$. The region of $z \to 1$ is automatically included in the evolution by the requirement that the integrated distribution must reproduce the DGLAP solution.

It is very interesting to observe, that the differences between the sets is very much reduced for heavy flavors, since they are generated dynamically, and the first term on the r.h.s of eq.(6) is absent for heavy flavors (since heavy flavors are not present at the starting scale in the VFNS which is applied here).

In Fig. 4 the transverse momentum distribution for down quarks, with and without including an intrinsic $k_{\rm T}$-distribution, is shown at different scales μ. While at low scales $\mu \sim 50$ GeV a significant effect of the intrinsic $k_{\rm T}$-distribution is observed for very small (not measurable) $k_{\rm T}$, at large scales $\mu \sim 350$ GeV this effect is much reduced. This scale depen-

DY mass spectrum over a large range on $m_{\rm DY}$ is obtained both with PB-NLO-2018 set 1 and set 2, only at $m_{\rm DY}$ greater than a few hundred GeV the predcitions tend to be too small; this is the region where the partonic x becomes large, and this is not well constrained by the fit to HERA data [20] used for the PB-NLO-2018 TMD extraction [19]. In the region of $m_{\rm DY}$ below the Z-pole one can observe the importance of QED corrections.

In Fig. 5(right) we show the photon transverse momentum spectrum in Z-production as measured by CMS [27] at 7 TeV in comparison with MCatNLO+CAS3 including QED radiation. The photon spectrum is well described at low $E_T < 40$ GeV, while the high E_T spectrum predicted by the parton shower falls below the measurement, as expected.

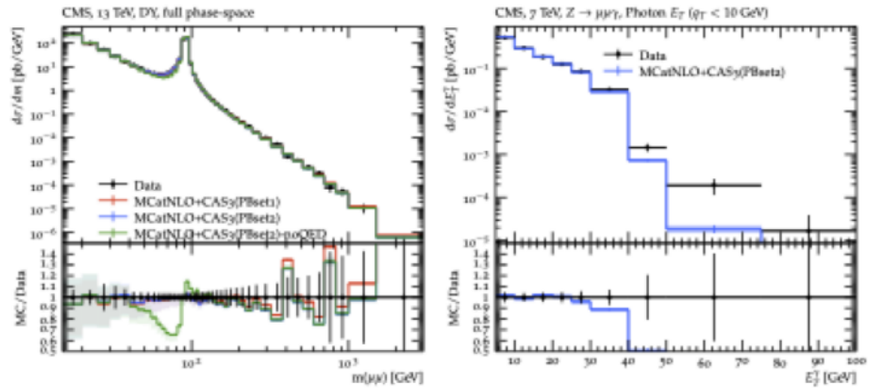

Figure 5: (Left): The mass distribution of DY lepton pairs at 13 TeV [25] compared to predictions of MCatNLO+CAS3 with PB-NLO-2018 set1, PB-NLO-2018 set2 and without QED corrections. (Right): The spectrum of photons in Z $\to \mu^+\mu^-\gamma$ at 7 TeV [27] compared to MCatNLO+CAS3 including QED radiation for a transverse momentum of the DY pair $q_t < 10$ GeV. The bands show the scale uncertainty.

4 The transverse momentum spectrum of DY lepton pairs

The transverse momentum spectrum of DY pairs at $\sqrt{s} = 13$ TeV has been measured for a wide $m_{\rm DY}$ range by CMS [21]. We will use this measurement for a comparison with predictions of MCatNLO+CAS3 based on PB-NLO-2018 set1 and PB-NLO-2018 set2, as shown in Fig. 6. The theoretical uncertainty is calculated from a variation of the renormalization and factorizations scales by a factor of two up and down avoiding the extreme combinations (7-point variation). As already observed in previous investigations [6, 7, 23, 28], the PB-NLO-2018 set1 gives to too high a contribution at small transverse momenta $q_{\rm t}$, while PB-NLO-2018 set2 describes the measurements rather well, without any further adjustment of

Intrinsic kt and soft region

parameters [†]. In order to illustrate the importance of QED corrections, we show in addition a prediction based on PB-NLO-2018 set2 without including QED final state radiation (labelled no-QED). Especially in the low m_{DY} region, the inclusion of QED radiation is essential, not only as a scale factor but it is rather strongly dependent on the transverse momentum $p_{\mathrm{T}}(\ell\ell)$. All predictions predict too low a cross section at large transverse momentum due to missing higher order contributions in the matrix element. For all further distributions we restrict the investigations to $p_{\mathrm{T}}(\ell\ell) < 30$ GeV.

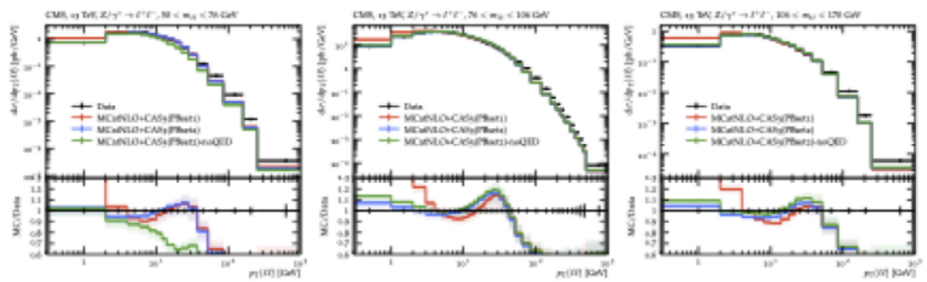

Figure 6: The $p_{\mathrm{T}}(\ell\ell)$ dependent DY cross section for different m_{DY} regions as measured by CMS [21] compared to MCatNLO+CAS3 predictions based on PB-NLO-2018 set 1 and set 2. Also show are predictions without inclusion of final state QED radiation off the leptons. The band shows the 7-point variation of the renormalization and factorization scale.

4.1 Influence of the intrinsic k_{T}-distribution

Given the rather successful description of the DY $p_{\mathrm{T}}(\ell\ell)$-spectrum with MCatNLO+CAS3 using PB-NLO-2018 set 2 in the low $p_{\mathrm{T}}(\ell\ell)$-region, we start now to investigate the importance of the intrinsic k_{T}-distribution. In PB-NLO-2018 the intrinsic k_{T}distribution is parametrized as a Gauss distribution with zero mean

$$\mathcal{A}_0(x, k^2_{\mathrm{T},0}, \mu_0^2) = f_0(x, \mu_0^2) \cdot \exp\left(-|k^2_{\mathrm{T},0}|/\sigma^2\right) \ , \tag{8}$$

with a width of $q_s = \sqrt{2}\sigma = 0.5$ GeV [19]. In order to illustrate the range of flexibility and the role of the intrinsic k_{T}-distribution, we show in Fig.7 MCatNLO+CAS3 predictions for the $p_{\mathrm{T}}(\ell\ell)$-spectrum of DY production at three different DY masses m_{DY} with the default gauss distribution as well as when no intrinsic k_{T} distribution is included (practically setting $q_s = 0.0001$ GeV). The overall effect of intrinsic k_{T}-distribution is rather small, only in the very low q_{t}-bins an effect of about five percent can be observed.

[†]The predictions shown here are slightly different compared to the predictions in [21] because we use here a lower minimum k_{T} cut and because of a bug in the treatment of QED radiation in Rivet

Treatment of systematic uncertainties

- χ^2 calculation with Covariance matrix representation C_{ik}

from HERAFITTER paper
Eur. Phys. J. C (2015) 75:304

$$\chi^2(\mathbf{m}) = \sum_{i,k}(m_i - \mu_i)C_{ik}^{-1}(m_k - \mu_k)$$

$$C_{ik} = C_{ik}^{stat} + C_{ik}^{uncorr} + C_{ik}^{sys}$$

  - this is the calculation used now: this is very new in data-MC comparison !

- χ^2calculation with nuisance parameter representation

$$\chi^2(\mathbf{m},\mathbf{b}) = \sum_i \frac{\left[\mu_i - m_i\left(1 - \sum_j \gamma_j^i b_j\right)\right]^2}{\delta_{i,unc}^2 m_i^2 + \delta_{i,stat}^2 \mu_i m_i\left(1 - \sum_j \gamma_j^i b_j\right)} + \sum_j b_j^2$$

  - with δ_i relative tat and uncorr syst uncertainty, $\gamma_j{}^i$, sensitivity of measurement to correlated sys source, and b_j, nuisance parameters, to be determined in fit

- both χ^2 definitions are not the same (?), but give a quantitative estimate of the deviation of the theory form the measurement

Schedule

- Small kt region in DY production
  - fits at 13 TeV are ongoing: Itana already has results with treatment of correlated systematics
  - fits at 8 TeV are ongoing: Sara has already good results
  - Fits need some further understanding, see next taks !

AOB

- Further news ?